

1 **Dilution of  $^{10}\text{Be}$  in detrital quartz by earthquake-induced landslides: implications for**  
2 **determining denudation rates and potential to provide insights into landslide**  
3 **sediment dynamics**

4  
5 A. Joshua West<sup>1\*</sup>, Ralf Hetzel<sup>2</sup>, Gen Li<sup>1</sup>, Zhangdong Jin<sup>3</sup>, Fei Zhang<sup>3</sup>, Robert G. Hilton<sup>4</sup>,  
6 and Alexander L. Densmore<sup>4,5</sup>

7  
8 <sup>1</sup> Department of Earth Sciences, University of Southern California, Los Angeles, CA 90089,  
9 United States

10 <sup>2</sup> Institut für Geologie, Westfälische Wilhelms-Universität, 48149 Münster, Germany

11 <sup>3</sup> State Key Laboratory of Loess and Quaternary Geology, Institute of Earth Environment,  
12 Chinese Academy of Sciences, Xi'an 710075, China

13 <sup>4</sup> Department of Geography, Durham University, Durham, DH1 3LE, United Kingdom

14 <sup>5</sup> Institute of Hazard, Risk and Resilience, Durham University, Durham, DH1 3LE, United  
15 Kingdom

16

17 \*corresponding author: [joshwest@usc.edu](mailto:joshwest@usc.edu)

18

19 Revised manuscript for consideration by *Earth and Planetary Science Letters*

## 20 **Abstract**

21 The concentration of  $^{10}\text{Be}$  in detrital quartz ( $^{10}\text{Be}_{\text{qtz}}$ ) from river sediments is now widely  
22 used to quantify catchment-wide denudation rates but may also be sensitive to inputs from  
23 bedrock landslides that deliver sediment with low  $^{10}\text{Be}_{\text{qtz}}$ . Major landslide-triggering events  
24 can provide large amounts of low-concentration material to rivers in mountain catchments,  
25 but changes in river sediment  $^{10}\text{Be}_{\text{qtz}}$  due to such events have not yet been measured directly.  
26 Here we examine the impact of widespread landslides triggered by the 2008 Wenchuan  
27 earthquake on  $^{10}\text{Be}_{\text{qtz}}$  in sediment samples from the Min Jiang river basin, in Sichuan, China.  
28 Landslide deposit material associated with the Wenchuan earthquake has  $^{10}\text{Be}_{\text{qtz}}$   
29 concentrations that are consistently lower than in river sediment prior to the earthquake.  
30 River sediment  $^{10}\text{Be}_{\text{qtz}}$  concentrations decreased significantly following the earthquake  
31 downstream of areas of high coseismic landslide occurrence, because of input of the  $^{10}\text{Be}$ -  
32 depleted landslide material, but showed no systematic changes where landslide occurrence  
33 was low. Changes in river sediment  $^{10}\text{Be}_{\text{qtz}}$  concentration were largest in small first-order  
34 catchments but were still significant in large river basins with areas of  $10^4$ - $10^5$  km<sup>2</sup>. Spatial  
35 and temporal variability in river sediment  $^{10}\text{Be}_{\text{qtz}}$  concentrations has important implications  
36 for inferring representative denudation rates in tectonically active, landslide-dominated  
37 environments, even in large basins. Although the dilution of  $^{10}\text{Be}_{\text{qtz}}$  in river sediment by  
38 landslide inputs may complicate interpretation of denudation rates, it also may provide a  
39 possible opportunity to track the transport of landslide sediment. The associated  
40 uncertainties are large, but in the Wenchuan case, the  $^{10}\text{Be}$  mixing suggests that river  
41 sediment fluxes in the 2-3 years following the earthquake increased by a similar order of  
42 magnitude in the 0.25-1 mm and the <0.25 mm size fractions, as determined from  $^{10}\text{Be}_{\text{qtz}}$   
43 mixing calculations and hydrological gauging, respectively. Such information could provide  
44 new insight into sediment transfer, with implications for secondary sediment-related hazards  
45 and for understanding the removal of mass from mountains.

46 **Keywords:** erosion; denudation; cosmogenic nuclides; landslides; Wenchuan earthquake;  
47 sediment

48

49 **Highlights:**

50 -  $^{10}\text{Be}$  concentrations in quartz measured in the region of the 2008 Wenchuan earthquake,  
51 China

52 - river sediment  $^{10}\text{Be}$  concentrations dropped due to input of landslide debris

53 -  $^{10}\text{Be}$ -denudation rate estimates should consider high-magnitude, low-frequency events

54 - effect of landslides on  $^{10}\text{Be}$ -denudation rates can be important even in large basins

55 - potential to infer sediment input from landslides and track its transport using  $^{10}\text{Be}$

## 56 1. Introduction

57 Accurately quantifying rates of erosion and sediment transport is vital to understanding mass  
58 redistribution processes at the Earth's surface, and how they relate to environmental and  
59 engineering hazards (e.g. Macklin and Lewin, 2003), regional to global-scale geodynamics  
60 and active tectonics (e.g. Willet, 1999; Attal and Lave, 2006; Parker et al. 2011), the  
61 biogeochemical systems that sustain life (e.g. Heimsath et al., 1997), and the function of the  
62 geological carbon cycle (e.g. West et al., 2005; Hilton et al., 2012). Over the past two  
63 decades, the use of cosmogenic radionuclides (CRNs) to determine denudation rates has  
64 provided a transformational new toolkit (Dunai, 2010), and the inventory of cosmogenic  
65  $^{10}\text{Be}$  produced *in-situ* in quartz grains ( $^{10}\text{Be}_{\text{qtz}}$ ) collected from river sediment is now widely  
66 used to infer denudation rates averaged over the area of river catchments and over  
67 timescales of  $10^2$  to  $10^4$  years (Granger et al., 1996; von Blanckenburg, 2006; Portenga and  
68 Bierman, 2010).

69  
70 In the  $^{10}\text{Be}_{\text{qtz}}$  approach, the concentration of  $^{10}\text{Be}$  in quartz grains is interpreted to reflect  
71 the integrated time that these grains have resided close to the Earth's surface. This is  
72 because  $^{10}\text{Be}$  production is attenuated at depth in the Earth due to cosmic ray interaction  
73 with rock material, so that the  $^{10}\text{Be}$  production rate is highest at the surface and decreases  
74 to negligible rates at a depth of several meters (e.g. Brown et al., 1995; Dunai, 2010). If the  
75 removal of material at the surface operates at a steady state, then determining the bulk  
76  $^{10}\text{Be}_{\text{qtz}}$  concentration in a sufficient number of detrital grains collected from river sediment  
77 can yield a representative catchment-averaged denudation rate (von Blanckenburg, 2006).  
78 Denudation rates determined in this manner are integrated over the time required for grains,  
79 on average, to move through the near-surface zone of  $^{10}\text{Be}$  production.

80

81 The supply of sediment from bedrock landslides may generate an important non-steady state  
82 perturbation to this averaging. This is because landslides can excavate material from both  
83 within and below the near-surface zone of  $^{10}\text{Be}$  production (Brown et al., 1995). By  
84 delivering shielded, low- $^{10}\text{Be}$  material to the river system, landslide sources are expected to  
85 dilute  $^{10}\text{Be}_{\text{qtz}}$  in river sediments (e.g. Niemi et al., 2005). These landslide inputs can  
86 potentially complicate accurate determination of denudation rates in tectonically-active  
87 settings, where information about erosion sheds valuable light on tectonic processes but  
88 where landslide erosion is frequently the dominant hillslope denudation mechanism (e.g.  
89 Hovius et al., 1997; Densmore et al., 1998). However, dilution of  $^{10}\text{Be}_{\text{qtz}}$  by bedrock  
90 landslide inputs may also present an opportunity to track the transport of landslide sediment  
91 through mountain catchments – an important problem from engineering, hazard, and science  
92 perspectives, but one that is non-trivial to tackle (e.g. Benda and Dunne, 1997; Cui et al.,  
93 2003a, 2003b; Dadson et al., 2004).

94  
95 The effects of stochastic and episodic landslide activity on river sediment  $^{10}\text{Be}_{\text{qtz}}$  have been  
96 considered theoretically (Niemi et al., 2005; Yanites et al., 2009; Ouimet, 2010), and some  
97 recent empirical measurements have confirmed that river sediment  $^{10}\text{Be}_{\text{qtz}}$  may be sensitive  
98 to stochastic inputs, e.g. from debris flows (Vassallo et al., 2011; Kober et al., 2012).  
99 However, there are little data to: (i) confirm in a systematic manner that landslide sources  
100 actually contribute material with relatively low concentrations of  $^{10}\text{Be}$  compared to  
101 background (pre-landslide input) values in river sediment; and (ii) assess how and to what  
102 extent the input of material as a result of a major landslide-triggering event may influence  
103 the  $^{10}\text{Be}_{\text{qtz}}$  signal in river sediments. In this study, we use the landslides triggered by the  
104 2008 Wenchuan earthquake in Sichuan, China, to address this problem, by measuring  $^{10}\text{Be}$   
105 concentrations both in landslide deposit material and in river sediment that has been  
106 influenced by input from this high-magnitude, low-frequency event. We compare our post-

107 earthquake river sediment  $^{10}\text{Be}_{\text{qtz}}$  data with results from samples collected at the same sites  
108 before the earthquake, and we explore the implications of the observed changes in  $^{10}\text{Be}_{\text{qtz}}$   
109 concentration for determining representative long-term denudation rates. We also consider  
110 the potential for the observed changes to contribute to understanding landslide sediment  
111 dynamics, although we acknowledge that the Wenchuan data leave large uncertainties in this  
112 application.

113

## 114 **2. Setting: The 2008 Wenchuan Earthquake and Landslides**

115 The  $M_w$  7.9 Wenchuan (or Sichuan) earthquake (Hao et al., 2008) occurred on May 12<sup>th</sup>,  
116 2008, along a series of dextral-thrust oblique-slip faults within the Longmen Shan, a  
117 mountain range that defines the eastern margin of the Tibetan Plateau and the  
118 northwestern edge of the Sichuan Basin. The earthquake triggered extensive coseismic  
119 landslides (e.g., Dai et al., 2010; Parker et al., 2011; Gorum et al., 2011; Xu et al., 2013;  
120 Ren et al., 2013; Li et al., 2014) and thus offers a valuable opportunity to explore the effect  
121 of widespread, impulsive delivery of landslide sediment to a fluvial network. Using remote  
122 sensing imagery collected over a time window of 1-6 months following the earthquake, we  
123 have recently produced a map of coseismic and immediately post-seismic landslides within  
124 the catchment area of the Min Jiang, which is the focus of this study (Fig. 1; Li et al.,  
125 2014). The Min Jiang is a principal tributary of the Yangtze River and one of the main  
126 rivers draining the Longmen Shan. It was the river with the largest drainage area to be  
127 acutely affected by Wenchuan earthquake-triggered landslides. The Min Jiang and its  
128 tributaries have incised deep valleys with high local relief (2-4 km) and steep slopes (angles  
129 often  $>30^\circ$ ) across the dramatic topographic gradient of the Longmen Shan, which rises  
130 from the Sichuan Basin at  $\sim 500$  m to peaks over 6000 m (Densmore et al., 2007; Ouimet et  
131 al., 2010; Zhang et al., 2011). The bedrock geology (Burchfiel et al. 1995; Robert et al.,  
132 2010; Burchfiel and Chen, 2012) is dominated by a Paleozoic passive margin sequence of

133 deformed metasediments intruded by granitic plutons, as well as Proterozoic granitoids and  
134 high-grade metamorphic rocks. The Heihe, Zagunao, and Yuzixi rivers, the major western  
135 tributaries of the Min Jiang, drain mainly granites and Songpan-Ganze flysch units, but show  
136 large contrasts in observed coseismic landslide areal density, defined here as area of landslide  
137 per unit catchment area (Fig. 1).

138

### 139 **3. Methods**

140 Following the Wenchuan earthquake, we collected samples from river sediments and  
141 landslide deposits for analysis of  $^{10}\text{Be}_{\text{qtz}}$ . For the landslide samples, we targeted a bedrock  
142 failure that is characteristic of the size of Wenchuan landslides and was accessible for sample  
143 collection from both the surface and interior of the deposit. In order to assess variability  
144 within landslide material, we collected two landslide sediment samples from different  
145 positions within the deposit (at the top of the surface and at the base of the deposit,  
146 exposed in cross section by road reconstruction) and one bedrock sample from the base of  
147 the exposed landslide scar. We targeted river sediment samples from sites where samples had  
148 been collected and analysed prior to the earthquake in 2004-2005 (Godard et al., 2010;  
149 Ouimet et al., 2009), with one additional sample from 2001 (Chappel et al., 2006). These  
150 sites included the Min Jiang River main stem, the Zagunao River, and the Yuzixi River, and  
151 2 small first-order sub-catchments (Fig. 1; Table 1). Two of the sites were sampled twice as  
152 part of this study, in March 2009 and April 2010, and the others were sampled once in April  
153 2010.

154

155 The stream and landslide sediment samples were washed, dried, and sieved into different  
156 grain-size fractions. To separate quartz for  $^{10}\text{Be}$  analysis, we used the 0.25–1 mm size  
157 fraction from all river sediments, and the 0.25–2 mm fraction for the landslide sediment  
158 samples (JWS 09-2 and JWS 09-3). To evaluate grain-size effects, we also analysed the 1–  
159 4 mm fraction in three of the river sediment samples. The bedrock sample from the landslide

160 scar was crushed and sieved to 0.25-1 mm size. The respective size fractions of each sample  
161 were split into magnetic and non-magnetic fractions with a hand magnet and a Frantz  
162 magnetic separator. The non-magnetic fraction was etched once in 6 M HCl and three to  
163 four times in diluted HF/HNO<sub>3</sub> in a heated ultrasonic bath to obtain clean quartz and  
164 remove any meteoric <sup>10</sup>Be (Kohl and Nishiizumi, 1992). Final purification of the quartz was  
165 achieved by two or three alternating etching steps in aqua regia and 8 M HF (Goethals et al.,  
166 2009). After addition of ~0.3 mg Be-carrier, 40–50 g of quartz from each sample was  
167 dissolved, and Be was separated on successive anion and cation exchange columns. The Be  
168 was precipitated as Be(OH)<sub>2</sub> and transformed to BeO at 1000°C. Targets were prepared for  
169 accelerator mass spectrometer (AMS) analysis at the AMS facility of ETH Zurich (Kubik  
170 and Christl, 2010).

171  
172 The areal density of landslides upstream of each river sediment sample was calculated from  
173 the landslide inventory mapped by Li et al. (2014) based on remote sensing imagery. Total  
174 landslide areas and areal densities were calculated as catchment-wide values, and as a  
175 function of proximity to the river sampling site. For the latter calculation, the catchment  
176 was divided into bands defined by 3 km increments along flow directions upstream from the  
177 sampling sites; landslide area and areal density were both calculated within each band in  
178 order to assess variability as a function of distance upstream from each sampling site.  
179 Catchment boundaries and areas, and flow direction and accumulation maps, were  
180 determined by flow routing using the hydrological algorithms in Grass GIS with SRTM  
181 digital elevation data (Jarvis et al., 2008).

182

#### 183 **4. Results**

184 <sup>10</sup>Be concentrations measured in quartz from the three samples from the landslide range  
185 from 0.17 to 2.14 × 10<sup>4</sup> at/g (Table 1) and decrease from the bottom of the landslide



186 deposit up to the base of the exposed scar (Fig. 2). Concentrations range from 1.16 to 3.65  
187  $\times 10^4$  at/g in river sediment, with generally but not universally higher concentrations in  
188 samples from the small first-order catchments when compared to the larger river basins.  
189 Concentrations are systematically slightly lower (by 15-20%) in the coarser (1-4 mm) size  
190 fraction compared to the finer (0.5-1 mm) size fraction where both fractions were analyzed  
191 from river sediments.

192  
193 Table 2 reports concentrations from samples collected after the Wenchuan earthquake (this  
194 study) and compares them to pre-earthquake data (Godard et al., 2010; Ouimet et al.,  
195 2009). The individual measurements for each sample time and site are shown graphically in  
196 Fig. 3. Only the data for the 0.25-1 mm size fraction are considered in this comparison,  
197 because complementary data on  $^{10}\text{Be}_{\text{qtz}}$  in larger size fractions of river sediment from before  
198 the earthquake are not available. Large differences between pre- and post-earthquake  
199 sediment  $^{10}\text{Be}_{\text{qtz}}$  (hereafter referred to as  $\Delta^{10}\text{Be}_{\text{qtz}} = ^{10}\text{Be}_{\text{qtz, preEQ}} - ^{10}\text{Be}_{\text{qtz, postEQ}}$ ) are  
200 observed. Four of the six sites show a post-earthquake decrease in  $^{10}\text{Be}_{\text{qtz}}$  that is greater  
201 than the reported analytical errors at the  $2\sigma$  level (Table 2; Figs. 3, 4). The two sites that  
202 do not show statistically significant  $\Delta^{10}\text{Be}_{\text{qtz}}$  (MJW and ZGN) at the  $2\sigma$  level are those that  
203 have relatively little coseismic landslide activity upstream of the sampling site (Table 3; Figs.  
204 3, 4). However,  $\Delta^{10}\text{Be}_{\text{qtz}}$  is not a simple function of landslide areal density within the  
205 catchment area upstream of each sampling site (Fig. 4a). Variability in  $\Delta^{10}\text{Be}_{\text{qtz}}$  is best  
206 explained if the location of landslides with respect to the basin outlet where sediments were  
207 collected is also considered (Table 3; Figs. 4b,c). For example, significant changes in  $^{10}\text{Be}_{\text{qtz}}$   
208 are observed for the main stem Min Jiang sampled near Yingxiu (site MJY), because of the  
209 very high landslide density immediately upstream of this sampling location (Fig. 4), even  
210 though the landslide density for the catchment as a whole is relatively low (Table 3).

211

212 Measured  $^{10}\text{Be}_{\text{qtz}}$  in the landslide samples is lower than in pre-earthquake river sediment, as  
213 expected theoretically, but falls in a similar range to post-earthquake river sediment. The  
214 highest of measured landslide  $^{10}\text{Be}_{\text{qtz}}$  is  $2.14 \pm 0.21 \times 10^4$  at/g. Seven out of the eight pre-  
215 earthquake samples from the large rivers of the Min Jiang system (see Table 3, and  
216 additional data from Godard et al., 2010) are between  $4.32 \pm 1.26$  and  $7.55 \pm 1.19 \times 10^4$  at/g,  
217 and the small catchment data (Ouimet et al., 2009) are even higher. One river sediment  
218 sample reported by Godard et al. (2010), LM261, has a  $^{10}\text{Be}$  concentration of  
219  $2.71 \pm 1.36 \times 10^4$  at/g. Although this value is still higher than our highest-concentration  
220 landslide sample, these two values cannot be distinguished statistically, given the  
221 uncertainties. However, the concentration reported for LM261 has an anomalously high  
222 uncertainty and is larger than the two other landslide samples we measured (at  
223  $0.95 \pm 0.12 \times 10^4$  at/g and  $0.17 \pm 0.07 \times 10^4$  at/g).

224

## 225 5. Discussion

### 226 5.1. Empirical confirmation of low $^{10}\text{Be}_{\text{qtz}}$ in landslide material

227 The observed  $^{10}\text{Be}_{\text{qtz}}$  in landslide material (Fig. 2) provide empirical data that confirm our  
228 expectations that Wenchuan landslides excavated shielded, low- $^{10}\text{Be}_{\text{qtz}}$  material via deep-  
229 seated failures. This is consistent with similar observations of low- $^{10}\text{Be}_{\text{qtz}}$  in landslides in  
230 Puerto Rico (Brown et al., 1995). Instantaneous excavation from depth yields relatively low  
231  $^{10}\text{Be}$  concentrations in the landslide sediment compared to pre-earthquake river sediment,  
232 because the latter (i) reflects material shed from hillslope surfaces that are  $^{10}\text{Be}$ -rich because  
233 of less rapid hillslope erosion during interseismic periods (Parker et al., 2011) and (ii) may  
234 have accumulated additional  $^{10}\text{Be}$  during fluvial transport to the sampling site (Anderson et  
235 al., 1996). The negligible  $^{10}\text{Be}$  inventory at the base of the exposed scar (Fig. 2) indicates  
236 near-complete shielding prior to failure at the estimated pre-excavation depths of  $>5\text{m}$   
237 where the scar was sampled. With only two data points, it is not clear whether the increase

238 from the top to the bottom of the deposit can provide any insight into failure dynamics (e.g.  
239 with material that previously resided at the hillslope surface, carrying relatively higher  $^{10}\text{Be}$   
240 concentrations, now at the bottom; see Fig. 2b). More systematic studies at higher  
241 resolution and on a greater number of landslides would be needed to explore this question.

242

## 243 **5.2. Implications for determining denudation rates**

244 The input of previously-shielded landslide debris with comparatively low  $^{10}\text{Be}_{\text{qtz}}$  is expected  
245 to decrease the  $^{10}\text{Be}_{\text{qtz}}$  in river sediment (Brown et al., 1995; Niemi et al., 2005; Yanites et  
246 al., 2009; Ouimet, 2010; Kober et al., 2012). Our data provide direct empirical  
247 demonstration of this effect associated with a single landslide-triggering event and suggest  
248 that, to first order, higher total areas and areal densities of landslides leads to larger  $\Delta^{10}\text{Be}_{\text{qtz}}$   
249 (Figs. 3, 4). Total landslide area ( $\text{km}^2$ ) and areal density (%) are not perfect metrics for  
250 actual input of landslide material into the river network, partly because of the location of  
251 landslides with respect to sampling sites (Fig. 4), and also because of variability in other  
252 factors including deposit grain size, depth of failure, and connectivity to the river channel  
253 network, which all may affect the extent to which a given landslide changes fluvial  $^{10}\text{Be}_{\text{qtz}}$ .  
254 Nonetheless, it is clear from our data (Figs. 3, 4) that sampling sites with only very small  
255 area of coseismic landslides in the upstream drainage do not show statistically significant  
256 changes in  $^{10}\text{Be}_{\text{qtz}}$ , while those sites with substantial upstream landslide areas showed  
257 significant decreases in  $^{10}\text{Be}_{\text{qtz}}$ .

258

259 These observations have important consequences for determining representative long-term  
260 erosion rates, because they mean that samples collected soon after a large event such as the  
261 Wenchuan earthquake may overestimate the actual magnitude of denudation rates over the  
262 timescales averaged by  $^{10}\text{Be}_{\text{qtz}}$ , while samples collected long after an event may  
263 underestimate rates. For example, at the Yuzixi sampling site (YZX), the  $^{10}\text{Be}$

264 concentrations in river sediment quartz collected before the earthquake implied erosion rates  
265 of  $0.64\pm 0.19$  and  $0.59\pm 0.17$  mm/yr, for samples from 2004 and 2005, respectively (Godard  
266 et al., 2010); immediately after the earthquake, the implied long-term rates would have been  
267  $1.20\pm 0.13$  and  $2.03\pm 0.35$  mm/yr (based on the  $^{10}\text{Be}_{\text{qtz}}$  measured in samples JWS 09-04 and  
268 JWS 10-19, and an analogous production scheme and erosion rate calculation to that used  
269 by Godard et al., 2010). Similar differences (approximately threefold increases) are implied  
270 for the Min Jiang main stem at Yingxiu (MJY) and for one of the small catchments (SCLX),  
271 while smaller differences in denudation rate (roughly 1.5- to 2-fold increases) are implied for  
272 sites ZGN and SCMJ. The actual long-term averaged rate may lie somewhere in between the  
273 values that would be inferred from pre- and post-earthquake samples (as suggested by  
274 Ouimet, 2010). Note that the implicit averaging timescale of the estimated denudation rate  
275 also changes, in the case of the YZS site from  $\sim 800$ -1350 years based on samples from  
276 before the earthquake, to  $\sim 250$ -550 years based on the post-earthquake samples.

277  
278 Models suggest that the input of landslide sediment may have a particularly significant effect  
279 on  $^{10}\text{Be}_{\text{qtz}}$  in catchments with small areas (Niemi et al., 2005; Yanites et al., 2009). Indeed,  
280 the small first-order catchments in this study show some of the largest  $\Delta^{10}\text{Be}_{\text{qtz}}$ , consistent  
281 with the greatest sensitivity to the rates and volumes of stochastic landsliding. The models  
282 also show that such stochastic effects should average to yield a representative long-term  
283 denudation rate for a sufficiently large catchment area. It is tempting to view the mean area  
284 at which model basins tend to become well-averaged ( $\sim 100$  km<sup>2</sup>; Niemi et al., 2005; Yanites  
285 et al., 2009) as a general threshold above which  $^{10}\text{Be}_{\text{qtz}}$  is likely to yield a robust denudation  
286 rate, even in settings prone to mass wasting. However, the significant  $\Delta^{10}\text{Be}_{\text{qtz}}$  seen in the  
287 large basins of the Min Jiang system, with catchment areas from 1000 to  $>10,000$  km<sup>2</sup>,  
288 indicates that cosmogenic nuclide samples from such large catchments may not necessarily  
289 always yield representative long-term denudation rates. This observation emphasizes that

290 there is a wide range around the mean value in the outputs of the stochastic models  
291 simulating landslide effects on river sediment  $^{10}\text{Be}_{\text{qtz}}$ . Moreover, these models make  
292 assumptions about landslides (e.g. magnitude-frequency relationships, area-volume scaling)  
293 that may be generally representative in a globally-averaged sense but are not always  
294 appropriate for all mountain belts. In particular, by averaging the effects of single high-  
295 magnitude, low-frequency earthquakes or storms that trigger large landslide pulses, the mean  
296 model outputs may underestimate the effect of events such as the Wenchuan earthquake.  
297 Thus very significant changes in the  $^{10}\text{Be}$  inventory may be expected in tectonically-active  
298 settings even in large river systems, especially where the recurrence time of major  
299 perturbations such as large earthquakes is long compared to the time it takes  $^{10}\text{Be}$   
300 concentrations to return to pre-event levels. The importance of such changes for long-term  
301 erosion rates will depend on return times of the high magnitude events.

302  
303 In principle, river sediment  $^{10}\text{Be}_{\text{qtz}}$  can also change over time when sediment source area  
304 changes, if different source areas have different characteristic  $^{10}\text{Be}_{\text{qtz}}$ . In mountain  
305 catchments, variability in source area  $^{10}\text{Be}_{\text{qtz}}$  is expected because elevation differences  
306 between tributaries lead to spatially variable  $^{10}\text{Be}$  production rates. Year-to-year changes in  
307  $^{10}\text{Be}_{\text{qtz}}$  from some rivers draining the south flank of the Nepalese Himalaya have been  
308 attributed to the location of rainfall events, which may selectively sample headwater  
309 sediment with variable  $^{10}\text{Be}_{\text{qtz}}$  (Lupker et al., 2012). These effects were not observed in the  
310 Min Jiang system prior to the Wenchuan earthquake, which instead showed constant  $^{10}\text{Be}_{\text{qtz}}$   
311 within uncertainty across multiple years (Godard et al., 2010). Moreover, sourcing effects are  
312 not likely to explain the observed post-earthquake changes in the Min Jiang, because these  
313 are observed across a range of scales (from small, first-order catchments to very large river  
314 basins) and are temporally and spatially associated with landslide occurrence.

315

316 The Wenchuan data also highlight the important role for the location of landslides relative  
317 to sampling sites in determining  $\Delta^{10}\text{Be}_{\text{qtz}}$  associated with an earthquake. Where landslide  
318 areal density is highest close the sampling site,  $\Delta^{10}\text{Be}_{\text{qtz}}$  is generally larger (Table 2, Figs. 3,  
319 4). Thus, in addition to potentially biasing the inferred magnitude of long-term denudation  
320 rates, landslide activity may introduce significant spatial heterogeneity that may or may not  
321 reflect actual spatial differences in denudation. Inferences about spatial variations in  
322 denudation rates, increasingly used to address fundamental questions about tectonic systems  
323 (e.g., Wobus et al., 2005; Densmore et al., 2009; Godard et al., 2012; Scherler et al., 2013;  
324 Godard et al., 2014), may in some cases be convoluted if spatial variability reflects the  
325 duration since the last major landslide-triggering event rather than more tectonically  
326 meaningful long-term denudation rates. The importance of such event-driven spatial  
327 variability is likely to depend on the return time and spatial distribution of landslide-  
328 triggering events, and on the recovery time of the erosional system. However, spatial  
329 variability in landslide occurrence may help to explain discrepancies in inferred erosion rates  
330 at different spatial scales in some regions. For example, in the case of the Longmen Shan,  
331 erosion rates inferred from cosmogenic nuclide measurements prior to the earthquake were  
332 significantly lower in small first-order catchments than in the Min Jiang main stem and its  
333 principle tributaries (Godard et al., 2010; Ouimet, 2010). The  $\Delta^{10}\text{Be}_{\text{qtz}}$  observed in this study  
334 as a result of the earthquake was larger for the small first-order catchments, bringing the  
335  $^{10}\text{Be}_{\text{qtz}}$  values for these small basins closer to the large river values, and suggesting that the  
336 pre-earthquake scale-discrepancy may have been at least in part related to the time since the  
337 last large event (as hypothesized by Godard et al., 2010 and Ouimet, 2010).

338

### 339 **5.3. $^{10}\text{Be}_{\text{qtz}}$ as a tracer of landslide-derived sediment**

340 Quantifying the post-earthquake transport of landslide-derived sediment has presented a  
341 major challenge in its own right. The magnitude, pattern and longevity of the sediment wave

342 from coseismic landslides have important implications for secondary hazards, because  
343 sediment chokes river channels, causes flooding and infrastructure damage, and clogs  
344 reservoirs (e.g., Huang and Fan, 2013). The transport of landslide sediment also influences  
345 large-scale orogenic processes, because removal of landslide debris is an important mass flux  
346 out of mountains (Hovius et al., 2011; Parker et al., 2011; Li et al., 2014). Most previous  
347 work on transport of landslide sediment has relied on measurements of suspended sediment  
348 fluxes collected at river gauging stations (e.g., in Taiwan: Dadson et al., 2004; Hovius et al.,  
349 2011; Yanites et al., 2010, 2011; in Sichuan: Wang et al., *in review*). This approach is  
350 limited by the available river gauging datasets and usually captures a selective grain size  
351 range. The dilution of  $^{10}\text{Be}_{\text{qtz}}$  by landslide material may provide an additional,  
352 complementary opportunity to trace the transport of landslide-derived sediment, but has not  
353 been previously explored.

354  
355 One possible approach for quantifying Wenchuan landslide inputs to the fluvial system is  
356 illustrated in Fig. 5. The mass of sediment being transported in the river following the  
357 earthquake ( $M_{\text{post}}$ ) can be calculated as a ratio to the pre-landslide sediment volume ( $M_{\text{pre}}$ )  
358 based on end-member mixing:

359  
360 
$$M_{\text{post}}/M_{\text{pre}} = (^{10}\text{Be}_{\text{qtz,pre}} - ^{10}\text{Be}_{\text{qtz,landslide}})/(^{10}\text{Be}_{\text{qtz,post}} - ^{10}\text{Be}_{\text{qtz,landslide}}) \quad (1)$$

361  
362 where  $^{10}\text{Be}_{\text{qtz,pre}}$  is the river sediment  $^{10}\text{Be}_{\text{qtz}}$  concentration before the earthquake (known for  
363 each site),  $^{10}\text{Be}_{\text{qtz,post}}$  is the river sediment  $^{10}\text{Be}_{\text{qtz}}$  concentration after the earthquake (also  
364 known for each site), and  $^{10}\text{Be}_{\text{qtz,landslide}}$  is the  $^{10}\text{Be}_{\text{qtz}}$  concentration of the landslide material.  
365  $^{10}\text{Be}_{\text{qtz,landslide}}$  is not precisely known because of variability in landslide material, both within  
366 and between landslides (cf. Fig. 2). Fig. 5 shows estimated  $M_{\text{post}}/M_{\text{pre}}$  as a function of the  
367 value of  $^{10}\text{Be}_{\text{qtz,landslide}}$ , for each of the sites in this study with significant  $\Delta^{10}\text{Be}_{\text{qtz}}$ . The

368 propagated analytical uncertainties lead to large possible ranges in  $M_{\text{post}}/M_{\text{pre}}$  but still clearly  
369 show that  $M_{\text{post}}/M_{\text{pre}}$  is much higher in some catchments (e.g. MJY, YZX) compared to  
370 others (ZGN), as expected based on the comparative  $\Delta^{10}\text{Be}_{\text{qtz}}$  values. Although the  
371 uncertainties are large, Fig. 5 could be used to make first-order quantitative estimates of  
372  $M_{\text{post}}/M_{\text{pre}}$ , given some constraints on  $^{10}\text{Be}_{\text{qtz,landslide}}$ .

373

374 It is not possible to directly measure the  $^{10}\text{Be}_{\text{qtz,landslide}}$  for the very large number (tens of  
375 thousands) of Wenchuan landslides. Instead, we approach this problem by modeling the  
376  $^{10}\text{Be}_{\text{qtz}}$  in each landslide using area-volume scaling relations and the theoretical decrease in  
377  $^{10}\text{Be}_{\text{qtz}}$  with depth below the Earth's surface (details described in Appendix A1). Estimated  
378 volume-averaged  $^{10}\text{Be}_{\text{qtz,landslide}}$  for all landslide material in each catchment (Table 3) ranges  
379 from  $1.24 \pm 0.12$  (for catchment MJY) to  $1.74 \pm 0.16 \times 10^4$  at/g (for catchment ZGN). These  
380 model-derived  $^{10}\text{Be}_{\text{qtz,landslide}}$  values provide a first-order constraint for estimating  $M_{\text{post}}/M_{\text{pre}}$   
381 for each catchment (Fig. 5).  $M_{\text{post}}/M_{\text{pre}}$  values inferred on this basis range from  $<2$  to  $>8$ ,  
382 depending on the catchment (Table 3). This ratio reflects an enhancement factor describing  
383 the increase in sediment mass in the river system as a result of landslide inputs, based on  
384 comparison before and after the earthquake. This  $^{10}\text{Be}$ -derived  $M_{\text{post}}/M_{\text{pre}}$  enhancement  
385 factor can be compared to the enhancement factor  $Q_{\text{ss-post}}/Q_{\text{ss-pre}}$ , calculated from the  
386 change in suspended sediment flux measured at gauging stations in the Min Jiang system  
387 before and after the Wenchuan earthquake (Wang et al., *in review*). For catchments where  
388 both datasets are available, the variability in  $M_{\text{post}}/M_{\text{pre}}$  values from one catchment to  
389 another closely mirrors the variability in  $Q_{\text{ss-post}}/Q_{\text{ss-pre}}$ , and although both ratios are  
390 associated with large uncertainties, the magnitude of the values for each catchment lie in  
391 similar ranges.  $M_{\text{post}}/M_{\text{pre}}$  describes the change in the mass of sediment in the river channel,  
392 while  $Q_{\text{ss-post}}/Q_{\text{ss-pre}}$  is the change in the mass flux of sediment per unit time that is  
393 transported by the river. It is perhaps not surprising that the two ratios would have similar



394 values, since the  $^{10}\text{Be}$  samples were collected from sediment deposits within the active river  
395 channel. An important difference is that  $M_{\text{post}}/M_{\text{pre}}$  has been determined from  $^{10}\text{Be}_{\text{qtz}}$  in the  
396 0.25-1 mm size fraction, while  $Q_{\text{ss-post}}/Q_{\text{ss-pre}}$  reflects predominantly material that is <0.25  
397 mm (Wang et al., *in review*). The overall similarity in the values of these ratios may suggest  
398 that there is not a strong grain size bias in terms of the entrainment and transport of  
399 material from Wenchuan landslides, at least within the range of sizes of the relatively fine-  
400 grained material considered here.

401  
402 The Wenchuan case illustrates that  $^{10}\text{Be}_{\text{qtz}}$  mixing may help to trace the transport of  
403 sediment from landslides, where these are sufficient in scale to measurably dilute the river  
404 sediment. This approach might be able to provide information where suspended sediment  
405 concentration data are lacking (e.g. in the small catchments SCLX and SCMJ in this study,  
406 see Table 3) and can offer insights into the transport of material across a range of size  
407 fractions that may be difficult to measure directly. Propagated uncertainties from the  $^{10}\text{Be}_{\text{qtz}}$   
408 mixing are large, but uncertainties from sediment flux estimates are also large (e.g. Dadson  
409 et al., 2004; Wang et al., *in review*). A main limitation of the  $^{10}\text{Be}_{\text{qtz}}$  mixing approach is  
410 that calculation of  $M_{\text{post}}/M_{\text{pre}}$  relies on the availability of  $^{10}\text{Be}_{\text{qtz}}$  data (or samples) collected  
411 before major landslide events, as well as after. For our study, the lack of data for the 1-4  
412 mm size fraction from prior to the earthquake prevents calculation of  $M_{\text{post}}/M_{\text{pre}}$  for this  
413 specific size range, although for the post-earthquake samples measured in this study,  
414 concentrations in the 1-4 mm size fraction are within 15-20% of those in the 0.25-1.0 mm  
415 size fraction. Replicating this experiment with larger grain sizes (including gravel and  
416 cobbles) could be an interesting next step.

417

418

419

#### 420 **5.4. Monitoring sediment removal by future $^{10}\text{Be}_{\text{qtz}}$ measurement**

421 The persistence of the sediment pulse from an event like the Wenchuan earthquake depends  
422 on the timescale of sediment transport through the system, in addition to the  $^{10}\text{Be}$   
423 concentrations associated with “background” (i.e., non-landslide) erosion and the associated  
424 background sediment production rates (e.g. Niemi et al., 2005). By monitoring changes in  
425  $^{10}\text{Be}_{\text{qtz}}$  following a major event, it may in principle be possible to determine the processes  
426 that govern the transport and eventual evacuation of the landslide sediment wave (e.g.  
427 Benda and Dunne, 1997). The rate of removal of landslide debris can be simplified by two  
428 idealized scenarios, in which removal is either limited by supply or by transport. These  
429 scenarios provide a useful conceptual framework for considering how the  $^{10}\text{Be}$  signal  
430 observed in this study in the Min Jiang might evolve with time in the future, at least to  
431 first-order.

432

433 We define *supply-limited removal* as occurring when the rate of removal of sediment  
434 material is determined by the volume that is available, in other words, when total change in  
435 volume  $V_{\text{ls}}$  is limited by the supply of landslide sediment to the fluvial network. This  
436 definition means that the volume of landslide material remaining within the Longmen Shan,  
437  $V_{\text{ls}}$ , at time  $t$  will depend on the volume of material available:

$$438 \quad dV_{\text{ls}}/dt = -kV_{\text{ls}} = -F_{\text{ls}} \quad (2)$$

439 where  $k$  is a constant and  $F_{\text{ls}}$  is the removal flux (i.e. the amount of sediment transported  
440 over time interval  $dt$ ). Equation 2 integrates to give:

$$441 \quad \Delta V_{\text{ls}} = V_{\text{ls}0} (1 - \exp(-kt)) \quad (3)$$

442 where  $V_{\text{ls}0}$  is the initial landslide volume following the earthquake (Fig. 6a). Sediment  
443 transport, on the other hand, should vary as the inverse of the total landslide volume (Fig.  
444 6b).

445

446 In contrast, we define *transport-limited removal* as occurring when the rate of removal of  
447 sediment is determined by the transport capacity of the fluvial network, which is determined  
448 by factors such as grain size and hydrological flow regime. In the theoretical end-member  
449 case, this removal rate would not depend on the amount of material available to transport,  
450 so would be independent of the volume of landslide debris remaining in the catchment. The  
451 change in volume with time thus becomes:

$$452 \quad dV_{ls}/dt = -F_{ls0} \quad (4)$$

453 where  $F_{ls0}$  is the removal flux immediately following the earthquake, yielding:

$$454 \quad V_{ls} = V_{ls0} - F_{ls0} t \quad (5)$$

455 as shown in Fig. 6a. These end-member definitions of supply- versus transport-limited  
456 sediment removal provide the basis for a simple, first-order model for the evolution of  
457 landslide sediment volumes and fluxes, and associated fluvial  $^{10}\text{Be}_{qtz}$ .

458  
459 Assuming a time window long enough to average flow conditions, and assuming that there  
460 are no long-term changes in flow conditions, the transport of material should take place  
461 within the space defined by the limits of the two end-member scenarios (see grey area in Fig.  
462 6a). The actual time-evolution of landslide volumes and associated sediment flux would  
463 theoretically be defined by some combination of the two. For example, the system may  
464 initially be transport-limited, because of the very large initial input of landslide debris into  
465 the river system, but once the initial supply of material in the rivers has been evacuated, the  
466 removal of the landslide material may become supply-limited. This shift might result from a  
467 grain size effect, as less material becomes available in a grain size range that can be  
468 mobilized under a given flow regime (e.g. Topping et al., 2000). It could also result from a  
469 topographic effect, because many landslide deposits are adjacent to river channels, so that  
470 the toe of the deposit enters the river system quickly while other parts of the deposit are less  
471 accessible for transport (e.g. the deposit in Fig. 2). Figs. 5b and 5c illustrate an example of

472 a possible trajectory in which sediment removal is initially transport-limited and then  
473 becomes supply-limited, but any number of possible combinations like this may be possible.  
474 Defining such trajectories assumes that additional supply from post-seismic landslides in  
475 years following the earthquake is small relative to the coseismic input. With post-seismic  
476 landslide maps, such additional sources could be taken into account explicitly (e.g., Hovius  
477 et al., 2011).

478  
479 The key point here is that the different scenarios for sediment transport have distinct  
480 implications for how they are expected to influence changes in river sediment  $^{10}\text{Be}_{\text{qtz}}$  with  
481 time (see Fig. 6c). Measurement of  $^{10}\text{Be}_{\text{qtz}}$  over time in the future may be able to shed light  
482 into what regulates the long-term removal of landslide debris following a major event such as  
483 the Wenchuan earthquake, while also providing quantitative insight into the longevity of the  
484 sediment pulse in the catchment system. For example, it would be valuable to know whether  
485  $^{10}\text{Be}_{\text{qtz}}$  concentrations remain low for an extended period of time (and if so, for how long)  
486 and then increase abruptly (supply-limited case), or if concentrations change more gradually  
487 over time (transport-limited case). Actual changes in  $^{10}\text{Be}_{\text{qtz}}$  in the future may be highly  
488 noisy, influenced by variable background erosion and sediment supply, and by stochastic  
489 processes such as source area changes (cf. Lupker et al., 2012), so it may not be possible to  
490 distinguish between transport scenarios. Still, first-order differences might be identifiable,  
491 and information on the pattern of these changes would be valuable for modeling post-  
492 earthquake sediment transport, with important implications for the persistence of sediment-  
493 related hazards.

494

## 495 **6. Conclusions**

496 Measurements of landslide deposits and river sediment from the Min Jiang river system  
497 provide direct empirical evidence that a major landslide-triggering event delivers low- $^{10}\text{Be}_{\text{qtz}}$

498 material to river systems, changing concentrations of  $^{10}\text{Be}$  in quartz in fluvial sediment. Such  
499 effects should be carefully considered when using cosmogenic nuclides to estimate  
500 denudation rates, even in large catchments (with areas of up to  $10^5 \text{ km}^2$ ), and when  
501 assessing spatial variability in these rates in settings where landslides are important erosional  
502 agents. Although the dilution of  $^{10}\text{Be}_{\text{qtz}}$  introduces complications for deriving information  
503 about denudation rates, it also has the potential to provide a new tool to trace the transport  
504 of landslide-derived sediment. Mixing calculations provide the opportunity to estimate the  
505 relative contribution of landslide material of differing grain sizes to the river sediment. The  
506 challenges in determining the representative  $^{10}\text{Be}$  concentrations in landslide material,  
507 together with the effect of propagated uncertainties, may be the primary limitation in the  
508 application of this approach, and more data from further studies will clearly be needed to  
509 test it rigorously. In the case of the Min Jiang and its tributaries, mixing calculations suggest  
510 that enhancement of sediment flux after the earthquake has been similar in the 0.25-1 mm  
511 bedload size fraction and in the suspended sediment (predominantly  $<0.25 \text{ mm}$ ) fraction. In  
512 addition to providing information about active transport processes, the capacity of  $^{10}\text{Be}_{\text{qtz}}$  to  
513 trace landslide sediment inputs may open the possibility of looking for variability in  $^{10}\text{Be}_{\text{qtz}}$  in  
514 sedimentary archives as a record of past variability in landslides and their triggers (e.g.,  
515 earthquakes). Further work would be needed to confirm whether variability in  $^{10}\text{Be}_{\text{qtz}}$   
516 obfuscates the signal associated with landslide sediment transport. Future applications are  
517 best suited to other systems where the scale of change in river sediment  $^{10}\text{Be}_{\text{qtz}}$  is likely to be  
518 as significant as in the Min Jiang, and this depends on factors such as event return time and  
519 magnitude, landslide spatial distribution, and catchment size (e.g. Niemi et al., 2005;  
520 Yanites et al., 2009).

521

522

523

524 **Acknowledgements**

525 This work was funded by NSF EAR-GLD Grant 1053504 to AJW, who received additional  
526 support from CAS YIS Fellowship 2011Y2ZA04. The research benefited from discussions  
527 with Niels Hovius, Vincent Godard, and Kate Huntington. Yi Long and Wei Fangqiang of  
528 the IMHE CAS, Chengdu, and Jin Wang at the IEE CAS, Xi'an, provided invaluable  
529 assistance for the fieldwork. We thank Anne Niehus for sample preparation and Peter Kubik  
530 (ETH Zurich) for the AMS measurements. The manuscript benefited significantly from  
531 constructive comments from two anonymous reviewers.

532 **Appendix A1: Calculating an estimated average  $^{10}\text{Be}$  composition of landslide**  
533 **material in each catchment**

534 Section 5.3 of the main text considers the question of using  $^{10}\text{Be}$  as a tracer of the amount  
535 of sediment material that has been input to the river system from coseismic landslides. This  
536 requires an estimate of the mass-weighted  $^{10}\text{Be}_{\text{qtz,landslide}}$  for each catchment area considered.  
537 In this appendix, we develop a model framework for calculating the  $^{10}\text{Be}_{\text{qtz}}$  in each landslide  
538 using area-volume scaling relations and the theoretical decrease in  $^{10}\text{Be}_{\text{qtz}}$  with depth below  
539 the Earth's surface. We then use the  $^{10}\text{Be}_{\text{qtz,landslide}}$  for each landslide to determine relevant  
540 values for each catchment.

541  
542 The area  $A$  of each landslide is known from mapping using remote-sensing imagery, and  
543 corresponding volume  $V$  is calculated based on power-law area-volume scaling ( $V = \alpha A^\gamma$ ),  
544 where  $\alpha, \gamma$  are parameters defined by global datasets ( $\log_{10}(\alpha) = -1.131, \gamma = 1.45 \pm 0.01$  from  
545 Guzzetti et al., 2009). Mean depth  $d$  for each landslide is determined as  $d = V/A$ .

546  
547 For the mapped location of each landslide (elevation, latitude, longitude), we calculate a  
548 theoretical steady-state  $^{10}\text{Be}_{\text{qtz}}$  vs depth curve. Assuming steady state denudation, the  $^{10}\text{Be}$   
549 concentration  $C$  at depth  $z$  (cf. Fig. 2b of the main text) can be represented as (Lal, 1991):

550 
$$C(z) = \sum_i \frac{P_i(0)}{\lambda + \rho \varepsilon / \Lambda_i} e^{-z\rho/\Lambda_i} \quad (\text{A1})$$

551 where  $i$  denotes each production pathway (neutrons and muons),  $P_i(0)$  is the production via  
552 pathway  $i$  at the surface (i.e.,  $z=0$ ),  $\lambda$  is the  $^{10}\text{Be}$  decay constant,  $\rho$  is the density of eroding  
553 rock,  $\varepsilon$  is the steady-state denudation rate, and  $\Lambda_i$  is the attenuation length associated with  
554 production pathway  $i$ . We use  $\rho=2.3 \text{ g/cm}^3$  and erosion rate  $\varepsilon$  defined by the measured pre-  
555 earthquake denudation rate in each catchment (from Ouimet et al., 2009; Godard et al.,  
556 2010). Here, we use two terms in Equation A1. For neutrons, we use  $\Lambda_n=160 \text{ g/cm}^2$  (a  
557 widely adopted value; cf. Goethals et al., 2009) and  $P_0$  calculated for the latitude, longitude,

558 and elevation of each landslide site based on scaling of a sea level high latitude production  
559 rate by neutrons of  $4.49 \text{ at g}^{-1} \text{ yr}^{-1}$  (Stone 2000; using code of Balco et al., 2008). For  
560 muons, we use  $\Lambda_m = 4200 \text{ g/cm}^2$  (the median value from the compilation of Braucher et al.,  
561 2013) and  $P_0$  calculated for the elevation of each landslide site based on scaling of a sea  
562 level high latitude production rate by neutrons of  $0.028 \text{ at g}^{-1} \text{ yr}^{-1}$  (Braucher et al., 2011,  
563 2013). We also calculated the results from Equation A1 with muonic production defined by  
564 the best fit to the depth-production trends of Heisinger et al. (2002a,b) using five  
565 exponential terms (e.g., Hidy et al., 2010); this muon production calculation leads to slightly  
566 different profiles of  $^{10}\text{Be}$  concentration vs. depth but does not change our overall conclusions.

567  
568 We sum the  $^{10}\text{Be}$  inventory over the depth above  $d$  (the landslide depth) and across area  $A$   
569 (landslide area) to give a total  $^{10}\text{Be}_{\text{qtz}}$  for each landslide. There are a number of assumptions  
570 in using Equation A1 to infer landslide  $^{10}\text{Be}_{\text{qtz}}$ . One is that the profile calculated using  
571 Equation A1 is for steady-state denudation; this may be valid if erosion rates have been  
572 constant at each landslide site over long enough time scale (approximately 2000-3000 years)  
573 to reach steady state, but would be violated if prior hillslope failure had cleared surface  
574 material within that time frame. Even if the depth profiles at each landslide site had reached  
575 steady state prior to the Wenchuan earthquake, we assume a spatial uniform denudation  
576 rate within each catchment, which is not likely to represent all landslide sites. However,  
577 spatial variability is expected to average over the very large number of landslides (100s to  
578 1000s) in each catchment. Our simple approach also ignores effects such as density  
579 differences, variability in the area-volume scaling relationship, topographic shielding of  
580 cosmic rays, and landslide geometry, all of which may vary from site to site. Nonetheless,  
581 our simple model provides a first-order estimate of the  $^{10}\text{Be}_{\text{qtz}}$  that might reasonably be  
582 expected for widely distributed landslides across the catchment areas. More data would  
583 clearly be needed to rigorously validate this approach, but for the one landslide with



584 measured concentrations, the predicted volume-averaged  $^{10}\text{Be}_{\text{qtz}}$  from our simple model is  
585  $1.17 \pm 0.16 / -0.13 \times 10^4$  at/g. Since the model result is based on theory, it is encouraging that  
586 the predicted average  $^{10}\text{Be}_{\text{qtz}}$  lies in the middle of the range of measured values for material  
587 from the landslide deposit, and that the predicted depth curve is consistent with the  
588 observed data (cf. Fig. 2 of main text).

589

590 To determine the volume-averaged  $^{10}\text{Be}_{\text{qtz,landslide}}$  for all landslide material in each catchment,  
591 we summed the  $^{10}\text{Be}$  inventory calculated for each landslide using Equation A1 and divided  
592 by the total volume of all the landslides in the catchment. For the large catchment sites  
593 (MJY, YZX, and ZGN), we restrict the analysis to landslides <50 km along flow directions  
594 from the sampling sites. This window captures the vast majority of landslides (Figs. 4b,c of  
595 main text) but excludes the landslides that are far from the sampling site and at very  
596 different latitudes and elevations, and are thus characterized by very different  $^{10}\text{Be}$   
597 production rates. A more complete sediment routing model would explicitly account for  
598 sediment transport distances and would be a valuable further research effort.

599 **References**

- 600 Anderson, R.S., Repka, J.L., Dick, G.S., 1996. Explicit treatment of inheritance in dating  
601 depositional surfaces using in situ  $^{10}\text{Be}$  and  $^{26}\text{Al}$ . *Geology* 24, 47–51.
- 602 Attal, M., Lavé, J., 2006. Changes of bedload characteristics along the Marsyandi River  
603 (central Nepal): Implications for understanding hillslope sediment supply, sediment load  
604 evolution along fluvial networks, and denudation in active orogenic belts. *Geological*  
605 *Society of America Special Papers* 398, 143–171.
- 606 Balco, G., Stone, J.O., Lifton, N.A., Dunai, T.J., 2008. A complete and easily accessible  
607 means of calculating surface exposure ages or erosion rates from  $^{10}\text{Be}$  and  $^{26}\text{Al}$   
608 measurements. *Quaternary Geochronology* 3, 174–195.
- 609 Benda, L., Dunne, T., 1997. Stochastic forcing of sediment supply to channel networks from  
610 landsliding and debris flow. *Water Resources Research* 33, 2849–2863.
- 611 Brown, E., Stallard, R., Larsen, M., Raisbeck, G., Yiou, F., 1995. Denudation rates  
612 determined from the accumulation of in situ-produced  $^{10}\text{Be}$  in the Luquillo experimental  
613 forest, Puerto Rico. *Earth and Planetary Science Letters* 129, 193–202.
- 614 Braucher, R., Bourlès, D., Merchel, S., Vidal Romani, J., Fernandez-Mosquera, D., Marti, K.,  
615 Léanni, L., Chauvet, F., Arnold, M., Aumaître, G., Keddadouche, K., 2013.  
616 Determination of muon attenuation lengths in depth profiles from in situ produced  
617 cosmogenic nuclides. *Nuclear Instruments and Methods in Physics Research Section B:*  
618 *Beam Interactions with Materials and Atoms* 294, 484–490.
- 619 Braucher, R., Merchel, S., Borgomano, J., Bourlès, D.L., 2011. Production of cosmogenic  
620 radionuclides at great depth: A multi element approach. *Earth and Planetary Science*  
621 *Letters* 309, 1–9.
- 622 Burchfiel, B., Chen, Z., Liu, Y., Royden, L., 1995. Tectonics of the Longmen Shan and  
623 adjacent regions, central China. *International Geology Review* 37, 661–735.
- 624 Burchfiel, B., Chen, Z., 2013. Tectonics of the Southeastern Tibetan Plateau and Its  
625 Adjacent Foreland. *Geological Society of America Memoirs* 210.
- 626 Chappell, J., Zheng, H., Fifield, K., 2006. Yangtse River sediments and erosion rates from  
627 source to sink traced with cosmogenic  $^{10}\text{Be}$ : Sediments from major rivers.  
628 *Palaeogeography, Palaeoclimatology, Palaeoecology* 241, 79–94.
- 629 Chmeleff, J., von Blanckenburg, F., Kossert, K., Jakob, D., 2010. Determination of the  $^{10}\text{Be}$   
630 half-life by multicollector ICP-MS and liquid scintillation counting. *Nuclear Instruments*

- 631 and Methods in Physics Research Section B: Beam Interactions with Materials and  
632 Atoms 268, 192–199.
- 633 Cui, Y., Parker, G., Lisle, T.E., Gott, J., Hansler-Ball, M.E., Pizzuto, J.E., Allmendinger,  
634 N.E., Reed, J.M., 2003a. Sediment pulses in mountain rivers: 1. Experiments. *Water*  
635 *Resources Research* 39, 1239, doi:10.1029/2002WR001803.
- 636 Cui, Y., Parker, G., Pizzuto, J., Lisle, T.E., 2003b. Sediment pulses in mountain rivers: 2.  
637 Comparison between experiments and numerical predictions. *Water Resources Research*  
638 39, 1240, doi:10.1029/2002WR001805.
- 639 Dadson, S., Hovius, N., Chen, H., Dade, B., Lin, J.-C., Hsu, M.-L., Lin, C.-W., Horng, M.-J.,  
640 Chen, T.-C., Milliman, J., Stark, C., 2004. Earthquake-triggered increase in sediment  
641 delivery from an active mountain belt. *Geology* 32, 733–736.
- 642 Densmore, A.L., Ellis, M.A., Anderson, R.S., 1998. Landsliding and the evolution of normal-  
643 fault-bounded mountains. *Journal of Geophysical Research* 103, 15203–15219.
- 644 Densmore, A.L., Ellis, M.A., Li, Y., Zhou, R., Hancock, G.S., Richardson, N., 2007. Active  
645 tectonics of the Beichuan and Pengguan faults at the eastern margin of the Tibetan  
646 Plateau. *Tectonics* 26, TC4005.
- 647 Densmore, A.L., Hetzel, R., Ivy-Ochs, S., Krugh, W.C., Dawers, N., Kubik, P., 2009. Spatial  
648 variations in catchment-averaged denudation rates from normal fault footwalls. *Geology*  
649 37, 1139–1142.
- 650 Dunai, T., 2010. *Cosmogenic Nuclides: Principles, Concepts and Applications in the Earth*  
651 *Surface Sciences*. Cambridge University Press, Cambridge.
- 652 Godard, V., Lavé, J., Carcaillet, J., Cattin, R., Bourlès, D., Zhu, J., 2010. Spatial  
653 distribution of denudation in Eastern Tibet and regressive erosion of plateau margins.  
654 *Tectonophysics* 491, 253–274.
- 655 Godard, V., Burbank, D.W., Bourlès, D.L., Bookhagen, B., Braucher, R., Fisher, G.B., 2012.  
656 Impact of glacial erosion on <sup>10</sup>Be concentrations in fluvial sediments of the Marsyandi  
657 catchment, central Nepal. *Journal of Geophysical Research* 117, F03013.
- 658 Godard, V., Bourlès, D.L., Spinabella, F., Burbank, D.W., Bookhagen, B., Fisher, G.B.,  
659 Moulin, A., Léanni, L., 2014. Dominance of tectonics over climate in Himalayan  
660 denudation. *Geology*, in press.
- 661 Goethals, M.M., Hetzel, R., Niedermann, S., Wittmann, H., Fenton, C.R., Kubik, P.W.,  
662 Christl, M., von Blanckenburg, F., 2009. An improved experimental determination of

- 663 cosmogenic  $^{10}\text{Be}/^{21}\text{Ne}$  and  $^{26}\text{Al}/^{21}\text{Ne}$  production ratios in quartz. *Earth and Planetary*  
664 *Science Letters* 284, 187–198.
- 665 Gorum, T., Fan, X., van Westen, C.J., Huang, R.Q., Xu, Q., Tang, C., Wang, G., 2011.  
666 Distribution pattern of earthquake-induced landslides triggered by the 12 May 2008  
667 Wenchuan earthquake. *Geomorphology* 133, 152–167.
- 668 Granger, D., Kirchner, J., Finkel, R., 1996. Spatially Averaged Long-Term Erosion Rates  
669 Measured from in Situ-Produced Cosmogenic Nuclides in Alluvial Sediment. *The Journal*  
670 *of Geology* 104, 249–257.
- 671 Guzzetti, F., Ardizzone, F., Cardinali, M., Rossi, M., Valigi, D., 2009. Landslide volumes and  
672 landslide mobilization rates in Umbria, central Italy. *Earth and Planetary Science Letters*  
673 279, 222–229.
- 674 Hao, K., Si, H., Fujiwara, H., Ozawa, T., 2009. Coseismic surface-ruptures and crustal  
675 deformations of the 2008 Wenchuan earthquake Mw7.9, China. *Geophysical Research*  
676 *Letters* 36, L11303, doi: 10.1029/2009GL037971.
- 677 Heimsath, A.M., Dietrich, W.E., Nishiizumi, K., Finkel, R.C., 1997. The soil production  
678 function and landscape equilibrium. *Nature* 388, 358–361.
- 679 Heisinger, B., Lal, D., Jull, A.J., Kubik, P., Ivy-Ochs, S., Neumaier, S., Knie, K., Lazarev,  
680 V., Nolte, E., 2002. Production of selected cosmogenic radionuclides by muons: 1. Fast  
681 muons. *Earth and Planetary Science Letters* 200, 345–355.
- 682 Heisinger, B., Lal, D., Jull, A.J.T., Kubik, P., Ivy-Ochs, S., Knie, K., Nolte, E., 2002.  
683 Production of selected cosmogenic radionuclides by muons: 2. Capture of negative  
684 muons. *Earth and Planetary Science Letters* 200, 357–369.
- 685 Hidy, A.J., Gosse, J.C., Pederson, J.L., Mattern, J.P., Finkel, R.C., 2010. A geologically  
686 constrained Monte Carlo approach to modeling exposure ages from profiles of  
687 cosmogenic nuclides: An example from Lees Ferry, Arizona. *Geochemistry Geophysics*  
688 *Geosystems* 11, Q0AA10. doi:10.1029/2010GC003084.
- 689 Hilton, R.G., Galy, A., Hovius, N., Kao, S.-J., Horng, M.-J., Chen, H., 2012. Climatic and  
690 geomorphic controls on the erosion of terrestrial biomass from subtropical mountain  
691 forest. *Global Biogeochemical Cycles* 26, GB3014. doi:10.1029/2012GB004314.
- 692 Hovius, N., Stark, C., Allen, P., 1997. Sediment flux from a mountain belt derived by  
693 landslide mapping. *Geology* 25, 231–234.

- 694 Hovius, N., Meunier, P., Lin, C.-W., Chen, H., Chen, Y.-G., Dadson, S., Horng, M.-J., Lines,  
695 M., 2011. Prolonged seismically induced erosion and the mass balance of a large  
696 earthquake. *Earth and Planetary Science Letters* 304, 347–355.
- 697 Huang, R., Fan, X., 2013. The landslide story. *Nature Geoscience* 6, 325–326.
- 698 Jarvis, A., Reuter, H.I., Nelson, E., Guevara, E., 2008. Hole-filled SRTM for the globe  
699 Version 4, available from the CGIAR-CSI SRTM 90m Database  
700 (<http://srtm.csi.cgiar.org>).
- 701 Kober, F., Hippe, K., Salcher, B., Ivy-Ochs, S., Kubik, P.W., Wacker, L., Hählen, N., 2012.  
702 Debris-flow-dependent variation of cosmogenically derived catchment-wide denudation  
703 rates. *Geology* 40, 935–938.
- 704 Kohl, C., Nishiizumi, K., 1992. Chemical isolation of quartz for measurement of in-situ -  
705 produced cosmogenic nuclides. *Geochimica et Cosmochimica Acta* 56, 3583–3587.
- 706 Korschinek, G., Bergmaier, A., Faestermann, T., Gerstmann, U.C., Knie, K., Rugel, G.,  
707 Wallner, A., Dillmann, I., Dollinger, G., von Gostomski, C.L., Kossert, K., Maiti, M.,  
708 Poutivtsev, M., Remmert, A., 2010. A new value for the half-life of  $^{10}\text{Be}$  by Heavy-Ion  
709 Elastic Recoil Detection and liquid scintillation counting. *Nuclear Instruments and*  
710 *Methods in Physics Research Section B: Beam Interactions with Materials and Atoms*  
711 268, 187–191.
- 712 Kubik, P.W., Christl, M., 2010.  $^{10}\text{Be}$  and  $^{26}\text{Al}$  measurements at the Zurich 6 MV Tandem  
713 AMS facility. *Nuclear Instruments and Methods in Physics Research Section B: Beam*  
714 *Interactions with Materials and Atoms* 268, 880–883.
- 715 Larsen, I.J., Montgomery, D.R., Korup, O., 2010. Landslide erosion controlled by hillslope  
716 material. *Nature Geoscience* 3, 247–251.
- 717 Li, G., West, A.J., Densmore, A.L., Jin, Z., Parker, R.N., Hilton, R.G., 2014. Seismic  
718 mountain building: Landslides associated with the 2008 Wenchuan earthquake in the  
719 context of a generalized model for earthquake volume balance. *Geochemistry Geophysics*  
720 *Geosystems* in press, doi:10.1002/2013GC005067.
- 721 Macklin, M.G., Lewin, J., 2003. River sediments, great floods and centennial-scale Holocene  
722 climate change. *Journal of Quaternary Science* 18, 101–105.
- 723 Niemi, N., Oskin, M., Burbank, D., Heimsath, A., Gabet, E., 2005. Effects of bedrock  
724 landslides on cosmogenically determined erosion rates. *Earth and Planetary Science*  
725 *Letters* 237, 480–498.

- 726 Nishiizumi, K., Imamura, M., Caffee, M.W., Southon, J.R., Finkel, R.C., McAninch, J., 2007.  
727 Absolute calibration of  $^{10}\text{Be}$  AMS standards. *Nuclear Instruments and Methods in*  
728 *Physics Research Section B: Beam Interactions with Materials and Atoms* 258, 403–413.
- 729 Ouimet, W., Whipple, K., Granger, D., 2009. Beyond threshold hillslopes: Channel  
730 adjustment to base-level fall in tectonically active mountain ranges. *Geology* 37, 579–582.
- 731 Ouimet, W.B., 2010. Landslides associated with the May 12, 2008 Wenchuan earthquake:  
732 Implications for the erosion and tectonic evolution of the Longmen Shan. *Tectonophysics*  
733 491, 244–252.
- 734 Ouimet, W., Whipple, K., Royden, L., Reiners, P., Hodges, K., Pringle, M., 2010. Regional  
735 incision of the eastern margin of the Tibetan Plateau. *Lithosphere* 2, 50–63.
- 736 Parker, R.N., Densmore, A.L., Rosser, N.J., de Michele, M., Li, Y., Huang, R., Whadcoat,  
737 S., Petley, D.N., 2011. Mass wasting triggered by the 2008 Wenchuan earthquake is  
738 greater than orogenic growth. *Nature Geoscience* 4, 449–452.
- 739 Portenga, E., Bierman, P.R., 2011. Understanding Earth's eroding surface with  $^{10}\text{Be}$ . *GSA*  
740 *Today* 21, 4–10.
- 741 Ren, Z., Zhang, Z., Dai, F., Yin, J., Zhang, H., 2013. Co-seismic landslide topographic  
742 analysis based on multi-temporal DEM--A case study of the Wenchuan earthquake.  
743 *SpringerPlus* 2, 544.
- 744 Robert, A., Pubellier, M., de Sigoyer, J., Vergne, J., Lahfid, A., Cattin, R., Findling, N., Zhu,  
745 J., 2010. Structural and thermal characters of the Longmen Shan (Sichuan, China).  
746 *Tectonophysics* 491, 165–173.
- 747 Scherler, D., Bookhagen, B., Strecker, M.R., 2013. Tectonic control on  $^{10}\text{Be}$ -derived erosion  
748 rates in the Garhwal Himalaya, India. *Journal of Geophysical Research Earth Surface*  
749 2013JF002955.
- 750 Stone, J.O., 2000. Air pressure and cosmogenic isotope production. *Journal of Geophysical*  
751 *Research* 105, 23753–23759.
- 752 Topping, D.J., Rubin, D.M., Vierra, L.E., 2000. Colorado River sediment transport: 1.  
753 Natural sediment supply limitation and the influence of Glen Canyon Dam. *Water*  
754 *Resources Research* 36, 515–542.
- 755 Vassallo, R., Ritz, J.-F., Carretier, S., 2011. Control of geomorphic processes on  $^{10}\text{Be}$   
756 concentrations in individual clasts: Complexity of the exposure history in Gobi-Altay  
757 range (Mongolia). *Geomorphology* 135, 35–47.

- 758 Von Blanckenburg, F., 2006. The control mechanisms of erosion and weathering at basin  
759 scale from cosmogenic nuclides in river sediment. *Earth and Planetary Science Letters*  
760 242, 224–239.
- 761 Wang, J., Jin, Z.D, Hilton, R.G., Zhang, F., Densmore, A.L., Li, G., West, A.J., *in review*.  
762 The chronic hazard of sediment mobilized by earthquake-triggered landslides in a  
763 continental mountain belt. *Geology*.
- 764 West, A.J., Galy, A., Bickle, M., 2005. Tectonic and climatic controls on silicate weathering.  
765 *Earth and Planetary Science Letters* 235, 211–228.
- 766 Wobus, C., Heimsath, A., Whipple, K., Hodges, K., 2005. Active out-of-sequence thrust  
767 faulting in the central Nepalese Himalaya. *Nature* 434, 1008–1011.
- 768 Xu, C., Xu, X., Yao, X., Dai, F., 2013. Three (nearly) complete inventories of landslides  
769 triggered by the May 12, 2008 Wenchuan Mw 7.9 earthquake of China and their spatial  
770 distribution statistical analysis. *Landslides* 1–21, doi: 10.1007/s10346-013-0404-6.
- 771 Yanites, B.J., Tucker, G.E., Anderson, R., 2009. Numerical and analytical models of  
772 cosmogenic radionuclide dynamics in landslide-dominated drainage basins. *Journal of*  
773 *Geophysical Research* 114, F01007, doi: 10.1029/2008JF001088.
- 774 Yanites, B.J., Tucker, G.E., Hsu, H.-L., Chen, C., Chen, Y.-G., Mueller, K.J., 2011. The  
775 influence of sediment cover variability on long-term river incision rates: An example from  
776 the Peikang River, central Taiwan. *Journal of Geophysical Research* 116, F03016.
- 777 Yanites, B.J., Tucker, G.E., Mueller, K.J., Chen, Y.-G., 2010. How rivers react to large  
778 earthquakes: Evidence from central Taiwan. *Geology* 38, 639–642.
- 779 Zhang, H., Zhang, P., Kirby, E., Yin, J., Liu, C., Yu, G., 2011. Along-strike topographic  
780 variation of the Longmen Shan and its significance for landscape evolution along the  
781 eastern Tibetan Plateau. *Journal of Asian Earth Sciences* 40, 855–864.

TABLE 1.  $^{10}\text{Be}$  concentrations in quartz from stream sediment and landslide deposit in the area of the 2008 Wenchuan earthquake, China

Sample ID	Description	Date of collection	Sample elevation (m)	Catchment elevation <sup>a</sup> (m)	Latitude (31°N)	Longitude (103°E)	Grain size (mm)	$^{10}\text{Be}$ concentration <sup>b</sup> ( $10^4$ at/g)	error <sup>c</sup> ( $1\sigma$ )
<b>Stream sediment samples</b>									
JWS 09-04	Yuzixi at Yingxiu	Mar-09	974	3545	03' 47.6"	28' 59.0"	0.25-1.0	2.34	±0.24
JWS 09-05	Min Jiang below Yingxiu	Mar-09	974	3491	02' 45.3"	28' 27.8"	0.25-1.0	1.58	±0.16
JWS 10-09	Same site as WBO-05-1 <sup>d</sup>	Apr-10	1568	2833	31' 31.5"	31' 11.0"	0.25-1.0	3.12	±0.36
JWS 10-10	Zagunao at Wenchuan	Apr-10	1351	3617	29' 23.2"	34' 49.4"	0.25-1.0	3.13	±0.33
JWS 10-11	Min Jiang above Wenchuan	Apr-10	1338	3516	28' 56.0"	36' 07.8"	0.25-1.0	3.25	±0.33
JWS 10-15	Same site as WBO-04-24 <sup>d</sup>	Apr-10	1409	2673	16' 05.2"	30' 48.5"	0.25-1.0	3.65	±0.35
JWS 10-19	Similar site to JWS 09-04	Apr-10	997	3545	04' 12.3"	28' 00.8"	0.25-1.0	1.38	±0.21
JWS 10-20	Similar site to JWS 09-05	Apr-10	974	3491	02' 42.7"	28' 28.2"	0.25-1.0	1.91	±0.23
JWS 10-09	Same as above	Apr-10	1568	2833	31' 31.5"	31' 11.0"	1.0-4.0	2.50	±0.29
JWS 10-10	Same as above	Apr-10	1351	3615	29' 23.2"	34' 49.4"	1.0-4.0	2.53	±0.31
JWS 10-19	Same as above	Apr-10	997	3545	04' 12.3"	28' 00.8"	1.0-4.0	1.16	±0.35
<b>Samples from landslide near Yingxiu</b>									
JWS 09-01	Bedrock sample from scar	Mar-09	1025	--	03' 56.3"	29' 6.7"	bedrock	0.17	±0.07
JWS 09-02	Top of landslide deposit	Mar-09	1016	--	03' 56.3"	29' 6.7"	0.25-2.0	0.95	±0.12
JWS 09-03	Base of landslide deposit	Mar-09	1011	--	03' 56.3"	29' 6.7"	0.25-2.0	2.14	±0.21

<sup>a</sup> Mean elevation of catchment upstream from sample location

<sup>b</sup> The blank-corrected  $^{10}\text{Be}$  concentrations are normalized to ETH standard S2007N, which has a nominal  $^{10}\text{Be}/^9\text{Be}$  ratio of  $28.1 \times 10^{-12}$  (Kubik and Christl, 2010) considering the  $^{10}\text{Be}$  half-life of 1.387 Ma (Chmeleff et al., 2010; Korschinek et al., 2010). The secondary standard S2007N has been calibrated to the primary standard ICN 01-5-1 (Nishiizumi et al., 2007; Kubik and Christl 2010)

<sup>c</sup> Propagated analytical errors ( $1\sigma$ ) include the error based on the AMS counting statistics and the error of the blank correction, but not the systematic uncertainty of the secondary standard S2007N, which is 2.7% (Kubik and Christl, 2010)

<sup>d</sup> Sample sites from Ouimet et al. (2009)



TABLE 2. Pre- versus post-earthquake  $^{10}\text{Be}$  concentrations in quartz from stream sediment

Site and sample	Date sample collected	$^{10}\text{Be}$ conc. ( $10^4$ at/g)	$1\sigma$ error ( $10^4$ at/g)
(A) Min Jiang at Yingxiu (MJY)			
Godard LM254 <sup>a</sup>	Spring 2004	6.03	0.86
Godard SC086 <sup>a</sup>	Fall 2005	5.02	1.52
JWS09-05	Spring 2009	1.58	0.16
JWS10-20	Spring 2010	1.91	0.23
	$\Delta^{10}\text{Be}$	<b>-3.78</b>	<b>0.39</b>
(B) Yuzixi at Yingxiu (YZX)			
Godard LM253 <sup>a</sup>	Spring 2004	4.49	0.88
Godard SC082 <sup>a</sup>	Fall 2005	4.88	0.92
JWS09-04	Spring 2009	2.34	0.24
JWS10-19	Spring 2010	1.16	0.35
	$\Delta^{10}\text{Be}$	<b>-2.94</b>	<b>0.79</b>
(C) Zagunao at Sangping (ZGN)			
Godard LM259 <sup>a</sup>	Spring 2004	4.32	1.26
JWS10-10	Spring 2010	3.13	0.33
	$\Delta^{10}\text{Be}$	<b>-1.19</b>	<b>1.30</b>
(D) Min Jiang above Wenchuan (MJW)			
Godard LM261 <sup>a</sup>	Spring 2004	2.71	1.36
JWS10-11	Spring 2010	3.25	0.33
	$\Delta^{10}\text{Be}$	<b>0.54</b>	<b>1.40</b>
(E) Small catchment on road to Lixian (SCLX)			
Ouimet WBO-05-1 <sup>b</sup>	2005	8.96	0.36
JWS10-09	Spring 2010	3.11	0.36
	$\Delta^{10}\text{Be}$	<b>-5.85</b>	<b>0.51</b>
(F) Small catchment along Min Jiang (SCMJ)			
Ouimet WBO-04-24 <sup>b</sup>	2004	6.65	0.34
JWS10-15	Spring 2010	3.65	0.35
	$\Delta^{10}\text{Be}$	<b>-3.00</b>	<b>0.49</b>

<sup>a</sup> Godard et al. (2010); <sup>b</sup> Ouimet et al. (2009).

TABLE 3. Landslide densities,  $\Delta^{10}\text{Be}$  values (for 0.25-1.0 mm grain size), and  $M_{\text{post}}/M_{\text{pre}}$  by catchment

Catchment	$\Delta^{10}\text{Be} \pm 1\sigma$ ( $10^4$ at/g)	$^{10}\text{Be}_{\text{qtz, landslide}}^{\text{a}}$ ( $10^4$ at/g)	$M_{\text{post}}/M_{\text{pre}}^{\text{b}}$	$Q_{\text{ss-post}}/Q_{\text{ss-pre}}^{\text{c}}$	Catchment area ( $\text{km}^2$ )	Landslide area ( $\text{km}^2$ )	Landslide areal density (%)	Max. incremental landslide density <sup>d</sup> (%)
(A) Min Jiang at Yingxiu (MJY)	-3.78±0.39	1.32 ( $^{+0.16}/_{-0.13}$ )	9.9 ( $^{+10.8}/_{-4.9}$ )	>6	21773	124.7	0.57	21
(B) Yuzixi at Yingxiu (YZX)	-2.94±0.79	1.15 ( $^{+0.13}/_{-0.12}$ )	5.9 ( $^{+4.0}/_{-2.7}$ )	4 to 6	1736	55.0	3.17	38
(C) Zagunao at Sangping (ZGN)	-1.19±1.30	1.94 ( $^{+0.22}/_{-0.20}$ )	2.0 ( $^{+0.9}/_{-0.7}$ )	1 to 2	4617	13.1	0.28	1.7
(D) Min Jiang above Wenchuan (MJW)	0.54±1.40	n.d. <sup>e</sup>	n.d. <sup>e</sup>	n.a. <sup>f</sup>	14210	12.4	0.09	9.6
(E) Small catchment on road to Lixian (SCLX)	-5.85±0.51	3.54 ( $^{+0.41}/_{-0.36}$ )	>10	n.a. <sup>f</sup>	19.69	0.32	1.63	–
(F) Small catchment along Min Jiang (SCMJ)	-3.00±0.49	2.64 ( $^{+0.30}/_{-0.27}$ )	4.0 ( $^{+1.8}/_{-1.0}$ )	n.a. <sup>f</sup>	41.37	1.60	3.87	–

<sup>a</sup> Model calculated, volume-weighted  $^{10}\text{Be}_{\text{qtz}}$  (mean  $\pm 1\sigma$ ) from landslides within the catchment area; see Appendix A1 for calculation method

<sup>b</sup> Based on mass balance for the 0.25-1.0 mm size fraction; calculated based on Fig. 5 for  $^{10}\text{Be}_{\text{qtz, landslide}}$  estimated for each catchment

<sup>c</sup> Based on change in suspended sediment yield that is dominated (>95%) by material <0.25 mm (Wang et al., *in review*)

<sup>d</sup> The maximum landslide areal density within 3 km distance contours along direction of flow from the sampling site (see Methods section of text)

<sup>e</sup> Not determined

<sup>f</sup> No gauging station data available

## Figure Captions

Figure 1. Map of the Min Jiang river basin in the Wenchuan earthquake region. Yellow polygons show landslides mapped by Li et al. (2014). Thicker river demarks the Min Jiang main stem. Stars are locations of river sediment samples for  $^{10}\text{Be}$  analysis, colour-coded by type of sample: reds – samples from Min Jiang main stem; oranges – large tributaries of the Min Jiang; blues – low-order catchments. Colours for each site match those used in Figures 3-5. Grey diamond is the landslide sample site. Abbreviations along rivers refer to catchments in this study: MJW – Min Jiang above Wenchuan, MJY – Min Jiang main stem near Yingxiu; YZX – Yuzixi sampled above Yingxiu; ZGN – Zagunao sampled above Wenchuan.

Figure 2. (a) Photograph of the landslide deposit sampled in this study, showing position of samples for  $^{10}\text{Be}_{\text{qtz}}$  analysis and measured values.  $^{10}\text{Be}_{\text{qtz}}$  concentrations are highest at the base of the landslide deposit, consistent with material previously residing closest to the surface, and lowest at the bottom of the exposed scar, as expected for material that was shielded from neutrons and muons prior to hillslope failure. (b) Sketch illustrating possible failure that would generate the observed variability in  $^{10}\text{Be}_{\text{qtz}}$  within the landslide scar and deposit, with predicted depth-variation based on model described in Appendix A1. More work on other landslides would be needed to determine if there are regular patterns in  $^{10}\text{Be}_{\text{qtz}}$  within landslide deposits that provide information about failure dynamics.

Figure 3. Concentrations of  $^{10}\text{Be}_{\text{qtz}}$  in river sediment from before (uncoloured bars) and after (coloured bars) the Wenchuan earthquake, from 6 different sites in the Min Jiang basin. Post-earthquake data were collected in this study from the 0.25-1 mm size fraction. Pre-earthquake data for the two small, first-order catchments are from Ouimet et al. (2009) who used the 0.25-0.50 mm size fraction; data for the larger rivers are from Godard et al. (2010)

who used the 0.25-1 mm size fraction. Our results show little size-dependence of  $^{10}\text{Be}_{\text{qtz}}$  within these ranges. Samples for the MJY site from Godard et al. (2010) were collected upstream of the confluence with the Yuzixi while JWS samples were taken downstream, but correction for the contribution from the Yuzixi based on erosion rate and aerial extent is negligible (<2%) because of the small Yuzixi basin area. Samples from locations downstream of high landslide areal density show significant changes in  $^{10}\text{Be}_{\text{qtz}}$  while samples further upstream show little change. The slight increase in  $^{10}\text{Be}_{\text{qtz}}$  of the Min Jiang at Wenchuan is not statistically significant, but if this is a real difference it may be due to natural variability or anthropogenic reworking of older sediments during reconstruction efforts following the earthquake. Both small catchments (blue colours) include significant areas of landslide activity within their boundaries. Note different scale for small catchments vs. large rivers; the change in  $^{10}\text{Be}_{\text{qtz}}$  after the earthquake decreases the discrepancy between large river and small catchment concentrations observed prior to the earthquake (see text).

Figure 4. (a) Landslide areal density plotted versus the change in  $^{10}\text{Be}_{\text{qtz}}$  concentrations of river sediment ( $\Delta^{10}\text{Be}_{\text{qtz}}$ ) from samples in the Min Jiang following the Wenchuan earthquake, compared to pre-earthquake values. Filled circles are for sites from the main stem and major tributaries; open circles from small first-order catchments. All sites with significant landslide activity show a decrease in measured  $^{10}\text{Be}_{\text{qtz}}$ , and this change is roughly correlated with the average landslide density in the catchment, although there is scatter in this correlation attributable at least in part to the location of landslides within each catchment, as shown in Figs. b and c. (b) Cumulative landslide density for each catchment, calculated for 3 km contours of distance along the flow direction upstream from the catchment outlet (see text). Highest cumulative landslide densities are close to the outlets, and the high peaks in landslide density correspond to large  $\Delta^{10}\text{Be}_{\text{qtz}}$ . (c) Landslide area in each catchment plotted as a function of the distance from the catchment outlet. Most landslides are close to the

catchment outlets; those catchments with greater concentrations of landslides near the outlet (slope of the curve in this plot) exhibit larger  $\Delta^{10}\text{Be}_{\text{qtz}}$ . In all cases catchment abbreviations are as in Tables 2 and 3.

Figure 5. Calculated ratio of the mass of river sediment after the earthquake relative to before ( $M_{\text{post}}/M_{\text{pre}}$ ) as a function of the average  $^{10}\text{Be}_{\text{qtz}}$  concentration of landslide inputs; see text for details. Colors are as in Figs 1, 3, & 4. Solid lines are the mean values; shaded regions show propagated  $1\sigma$  uncertainty envelopes bounded by dashed lines.

Figure 6. A schematic illustration of the theoretical time evolution through a major landslide event followed by recovery, illustrating the idealized conceptual end-member cases for supply-limited and transport-limited removal of landslide debris. Actual system evolution is likely to reflect some combination of supply and transport limits, as illustrated in the grey region in (a) and by the example curve in (b) and (c). Note that many different actual curves might be possible; this is just one possibility as an illustration. (a) Evolution of landslide volume remaining in the catchment over time; (b) evolution of fluvial sediment flux; and (c) implications for  $^{10}\text{Be}$  concentration in quartz from fluvial sediments. In the case of an event like Wenchuan, where  $^{10}\text{Be}_{\text{qtz}}$  data is available from before and after the earthquake, monitoring in the future might provide an opportunity to understand what controls sediment evacuation by comparison to these theoretical trajectories.

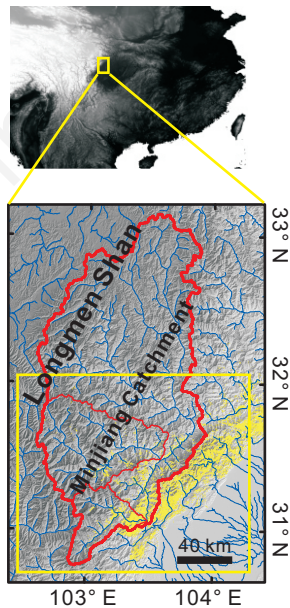
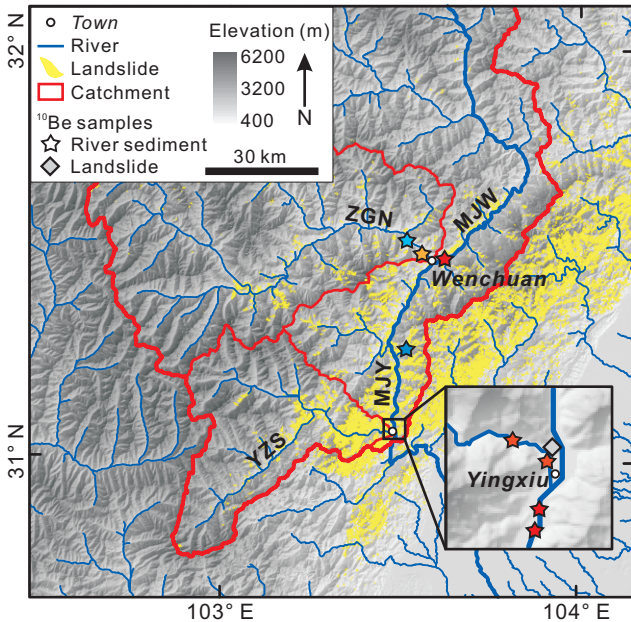


FIGURE 1

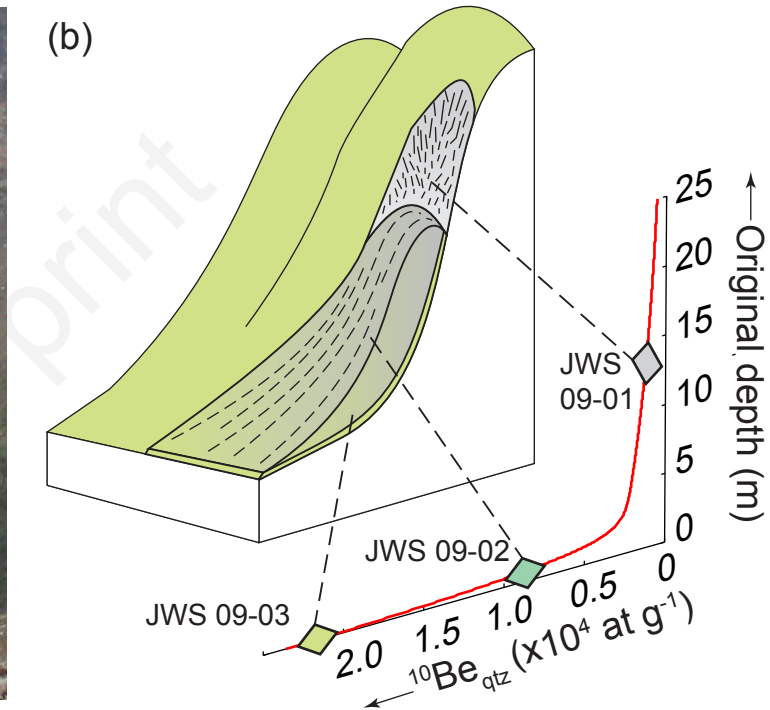
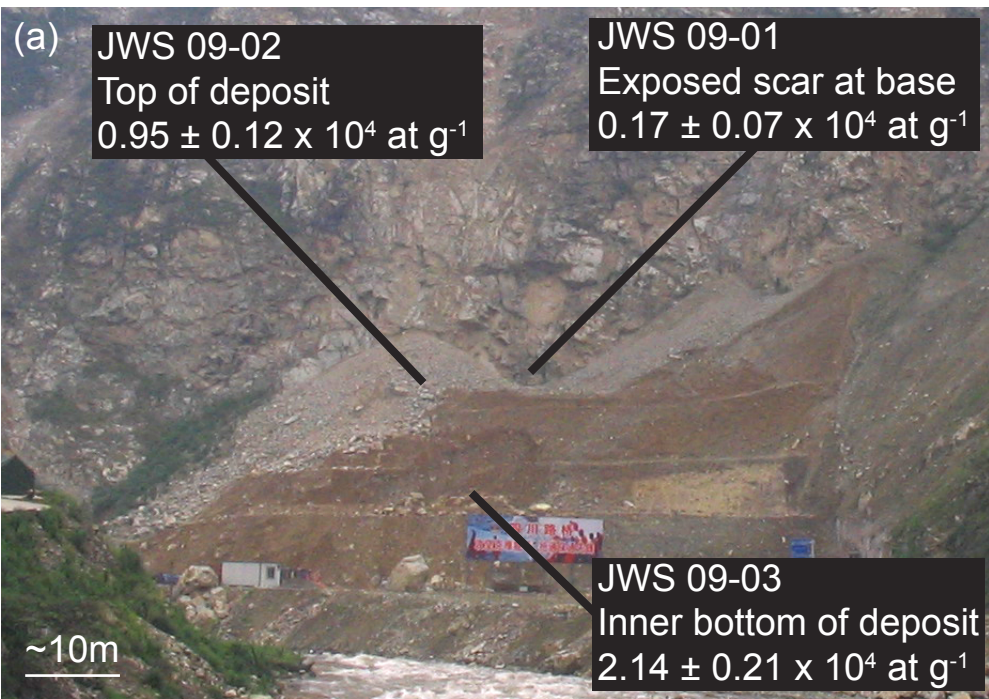


FIGURE 2

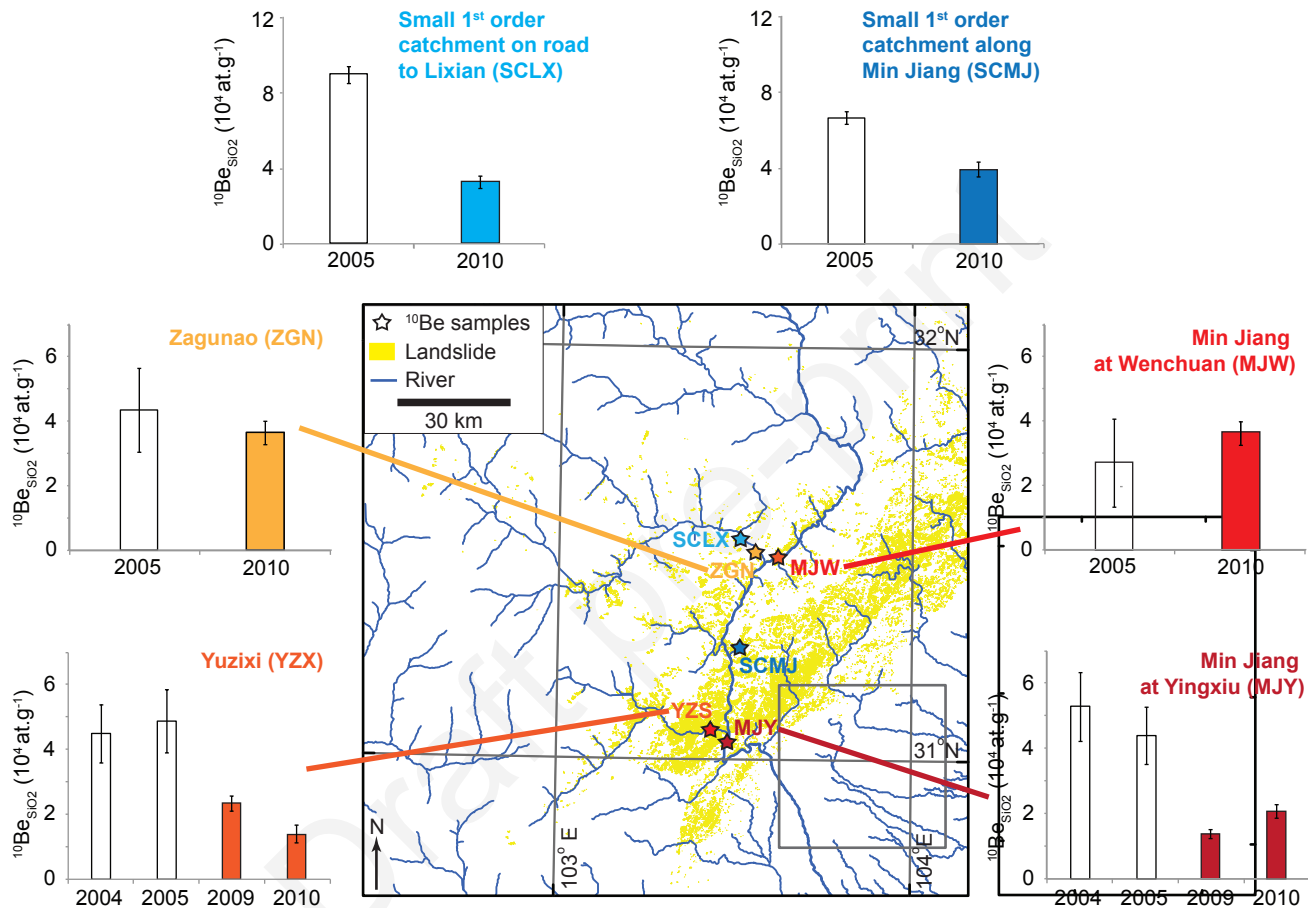


FIGURE 3



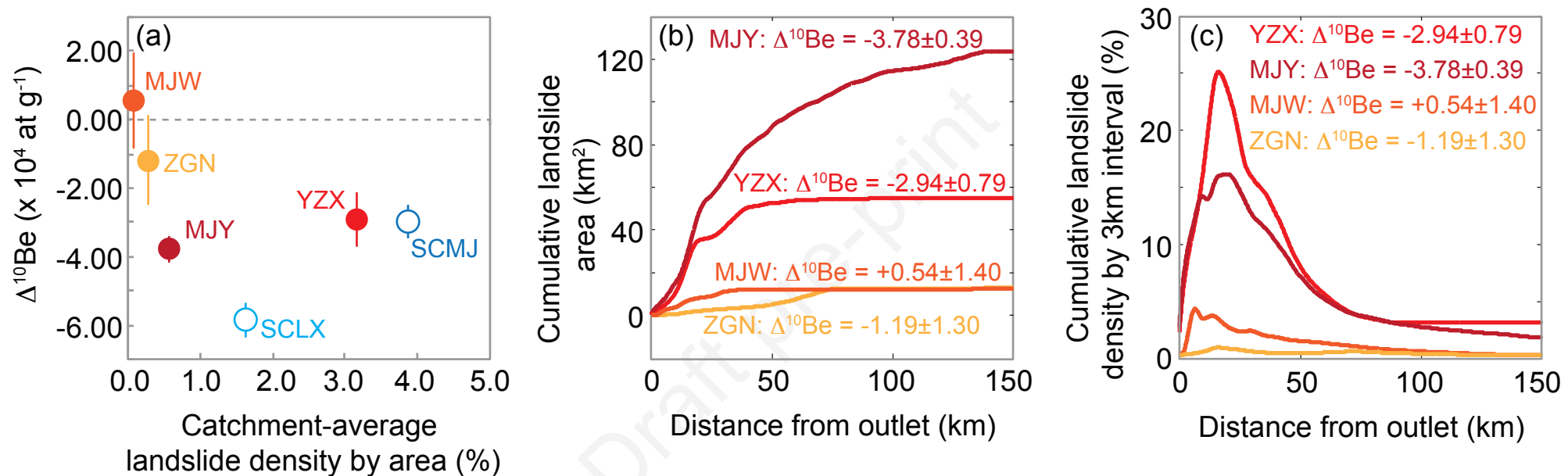


FIGURE 4

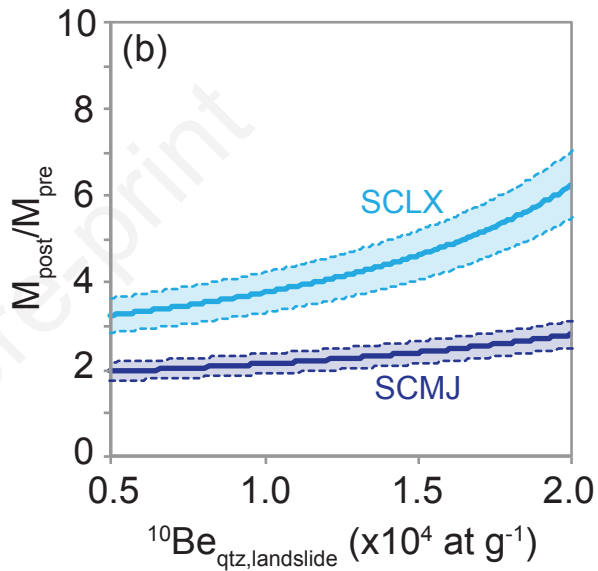
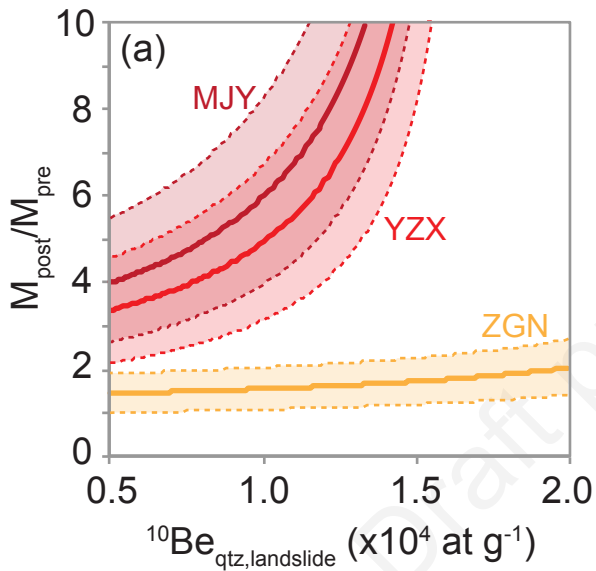


FIGURE 5

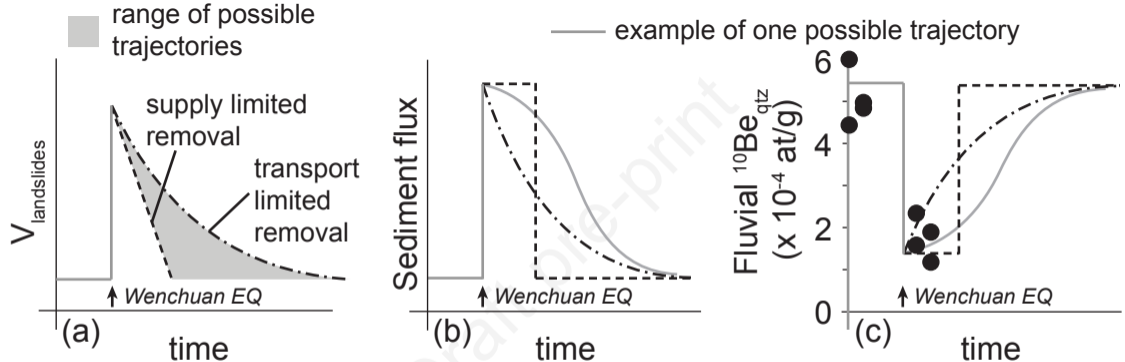


FIGURE 6